

# Disentangling the role of structure and friction in shear jamming

H. A. Vinutha and Srikanth Sastry\*

*Jawaharlal Nehru Center for Advanced Scientific Research,*

*Jakkur Campus, Bangalore 560064, India and*

*TIFR Center for Interdisciplinary Sciences,*

*21 Brundavan Colony, Narsingi, 500075 Hyderabad, India*

## Abstract

Amorphous packings of spheres have been intensely investigated in order to understand the mechanical and flow behaviour of dense granular matter, and to explore universal aspects of the transition from fluid to structurally arrested or jammed states. Considerable attention has recently been focussed on anisotropic packings of frictional grains generated by shear deformation leading to *shear jamming*, which occurs below the jamming density for isotropic packings of frictionless grains. With the aim of disentangling the role of shear deformation induced structures and friction in generating shear jamming, we study sheared assemblies of *frictionless* spheres computationally, over a wide range of densities, extending far below the isotropic jamming point. We demonstrate the emergence of a variety of geometric features characteristic of jammed packings with the increase of shear strain. The average contact number and the distributions of contact forces suggest the presence of a threshold density, well below the isotropic jamming point, above which a qualitative change occurs in the jamming behaviour of sheared configurations. We show that above this threshold density, friction stabilizes the sheared configurations we generate. Our results thus reveal the emergence of geometric features characteristic of jammed states as a result of shear deformation alone, while friction is instrumental in stabilising packings over a range of densities below the isotropic jamming point.

---

\* Kavli Institute of Theoretical Physics, Kohn Hall, University of Santa Barbara, CA 93106-4030, USA

The transition from a fluid to a rigid, or jammed, state occurs and is of interest in a wide variety of condensed matter, with glasses, granular packings and colloidal suspensions being well known examples. Understanding the transition, occurring variously when temperature or applied stress is lowered, or the density raised, involves interconnected changes in structure, thermodynamics, dynamics of structural relaxation and rheology, and a unified and definitive picture of this *jamming* transition, has been an actively pursued goal with implications in diverse areas of research [1]. Random packings of frictionless hard and soft spheres have been studied in this general context [1–4], and in particular as an idealised or *reference* model for granular materials. Much attention has been focussed on behaviour as the jamming point, identified [2, 3] to occur as a packing fraction of about 64%, is approached. Although the density at which *random close packing* occurs is understood not to be unique (see, *e. g.*, [1, 4, 5] and references therein), many aspects of behaviour suggesting the jamming point (denoted henceforth as  $\phi_J$ ) to be a *critical* point[6], appear robust [1]. Real granular materials studied experimentally inevitably deviate from this idealization, and how these deviations influence their jamming behaviour has been an active subject of recent research[7–12]. In particular, jamming of frictional grains under shear deformation, or *shear jamming*, has been shown to arise [9] over a range of stresses, and of densities below  $\phi_J$ , resulting in a density-stress *phase diagram* that is substantially different from the frictionless case [13]. An extended range of jamming densities has also been discussed earlier in the context of *random loose packing* [2, 3, 14], protocol dependence [15], and memory effects [16], and specifically for frictional packings [7, 8]. Given that the structural changes and organisation resulting from the shear deformation, as well as friction likely play an important role in generating shear jammed packings, elucidating the role of each of these factors is central to understanding shear jamming. We address this issue here, through a computational study of sheared configurations of frictionless soft spheres.

We study a system of  $N = 2000$  equal-sized frictionless spheres interacting with a harmonic repulsive potential [5, 6] over a wide range of densities, from a packing fraction of 0.26 to 0.627, generated (for high densities) by rapid compression of fluid configurations or decompression of jammed configurations. Shear deformation is applied through an athermal quasi static procedure [13], by incrementing strain  $\gamma_{xz}$  in small steps (typically of  $d\gamma = 5 \times 10^{-5}$ , but as low as  $d\gamma = 5 \times 10^{-12}$  in cases indicated), followed by energy minimisation at each step. The procedure is applied till a steady state in which the shear stress  $\sigma_{xz}$  (which

remains very small) and the average number of contacts  $Z$  reach stable values. Further details concerning the simulations and analysis are presented in Methods and Supplementary Information (SI).

We monitor the evolution of the structure under shear by considering the pair correlation function  $g(r)$ , the distribution of the number of contacts each sphere has, and the free volume distribution, each of which exhibit unique signatures near the jamming point for frictionless sphere packings: The pair correlation function exhibits a near-contact power law singularity  $g(r) \sim (\frac{r}{\sigma} - 1)^{-\gamma}$  and singularities in the (split) second peak [17, 18]. The contact number distribution, which we compute with and without considering rattlers (rattlers are spheres with fewer than 4 contact neighbors), is peaked at  $Z = 6$ , the value required by the isostaticity condition. The free volumes of individual spheres are computed using an exact algorithm that employs the Voronoi tessellation, and the free volume distribution exhibits a distinct power law tail for nearly jammed packings, as described [19] and references therein. This feature of the free volume distribution has also been observed for sheared configurations in two and three dimensions at high densities close to the jamming point [20]. In Fig. 1, we show how these features evolve, for sheared configurations at different values of strain for packing fraction  $\phi = 0.58$ . It is seen that the  $g(r)$  develops a near contact power law [17, 18], initially absent, as shear strain is increased (Fig. 1(a)), and the split-second peak develops the characteristic twin singularities (Fig. 1(b)) [18]. The peak of the distribution of contact numbers, initially at zero, evolves to larger values. Finally, the free volume distribution, initially exhibiting a form typical of the fluid, develops a power law tail characteristic of nearly jammed packings [19]. Thus, sheared fluid configurations at  $\phi = 0.58$  develop, by all these measures, characteristics of jammed configurations. Fig. 2 shows the same quantities in the steady state, for the range of densities studied, demonstrating the same behaviour at all densities. While the near contact power law in the  $g(r)$  is very similar in all cases, the sub-peak at smaller  $r$  in the second peak, as may be expected from packing considerations, becomes sharper as density increases. The average number of contacts moves from values less than 4 towards 6 as density increases. Table I summarises information on contact numbers. The exponent in the free volume distribution changes slightly with density, as does the exponent describing the near contact in  $g(r)$ . Although these variations require explanation, the main point is clear: with an increase of shear strain, initially fluid configurations over a broad range of densities evolve structures that bear strong resemblance

to jammed configurations.

We consider next the statistics of the number of contacts and the distribution of forces between spheres. In Fig. 3 (a), we show the parametric relationship between the mean contact number and the density that we have of our sheared configurations of frictionless spheres. The mean contact number decreases from a 6 at the isotropic frictionless jamming density of  $\sim .64$ , to a value of 4 at a density  $\sim 0.55$ . Interestingly, the relationship displayed by our data closely matches those of [7, 8], for frictional jammed packings. The presence of a threshold density of 0.55 is further supported by the distribution of contact forces normalised to their mean value,  $P(f)$ , shown in Fig. 3 (b). These distributions show a peak at finite values above  $\phi = 0.55$ , a previously identified characteristic of jammed packings [21–23]. These results together indicate the presence of a threshold density 0.55, and a similarity between the sheared configurations of frictionless spheres we generate and frictional jammed packings. This observation has resonance with a number of other past suggestions, including the occurrence of a glass transition [25], shear thickening [26], onset of dilatancy and random loose packing [14]. The last of these, random loose packing, however, is a feature of frictional packings, and we have so far dealt with frictionless packings. An appealing picture, which we explore below, is that shear deformation, even in the absence of friction, serves to induce structures [27] at densities above 0.55, and considerably below  $\phi_J$ , which may be stabilised by friction, when present, to produce shear jammed packings.

Before we consider the role of friction, we consider the jamming properties of the sheared frictionless packings themselves, by applying the Lubachevsky-Stillinger [24] jamming procedure (see Methods) for a range of compression rates to the configurations generated at different densities. For slow compression rates, for all initial densities, the resulting jammed configurations have densities close to  $\phi = 0.64$ , as seen in Fig. 3 (c). However, at high compression rates, we note a difference in behaviour across  $\phi \sim 0.58$ . At higher initial densities, configurations jam at roughly the same density, while at lower initial densities, the jammed densities are higher. The possibility of generating jammed configurations above a density of 0.58, albeit at high compression rates, appears related to the percolation of locally stable structures. In Fig. 3 (d) we show the percolation probability of spheres with contact number  $Z \geq 2D = 6$ , for different system sizes  $N = 256, 2000, 5000$ . The connected clusters of such spheres percolations at  $\sim 0.58$ . The suggested possibility of 0.58 being a threshold that is distinct from that at density 0.55, and the analysis of other percolation characteristics that

may elucidate the limiting density of 0.55 suggested by other results above, deserve further analysis but are not pursued further here. Percolation of  $D + 1$  coordinated spheres occurs at a much lower density, data for which is shown in the SI for completeness.

In order to assess whether sheared frictionless spheres can jam in the presence of friction, we perform simulations including frictional contact forces using the discrete element method (DEM). We subject the steady state sheared configurations to a strain step ( $d\gamma = 5 \times 10^{-5}$ ) in addition to slight compression (see Methods and SI), and evolve them using DEM, varying the friction coefficient  $\mu$  and the damping coefficients  $\zeta_n$  and  $\zeta_t$  (see Methods and SI), and monitor the evolution of the structure. We initially choose damping coefficients  $\zeta_n = \zeta_t = 0$ . Although the spheres do not move significantly during any of these simulations (with mean squared displacements less than  $10^{-4}$ ), for small enough friction coefficients at any density, the shear stress and the average contact number decay rapidly to zero indicating that the structure is unjammed (see SI). The threshold friction coefficient is identified at each density beyond which the sheared configurations remain jammed. For densities above  $\phi = 0.58$ , sheared configurations remain jammed, while below, the configurations unjam for the studied range of friction coefficients. Fig. 4(a) shows the threshold friction coefficients obtained, which compare reasonably well with values obtained in frictional simulations by Silbert [8]. Fig. 4 (b) shows the fraction of initial contacts that survive as a function of time, for large friction coefficients well above the threshold value, with steady state configurations generated with  $d\gamma = 10^{-12}$ . It is seen that most of the contacts remain intact for densities above  $\phi = 0.57$ , while they decay to 0 below. A closer agreement with frictional simulations by Silbert [8] are obtained by the inclusion of damping (as done in [8]), as shown in Fig. 4(a). For  $\zeta_n = 3$  and 30 ( $\zeta_t = \frac{1}{2}\zeta_n$ ) respectively, frictional jamming occurs down to  $\phi = 0.58$  and 0.57. The mean contact number  $Z$ , at the lower density limit to frictional jamming reaches 4 in all these cases as shown in Figure 4(c). With a suitable procedure, we therefore expect the lower density limit to frictional jamming to be  $\phi = 0.55$ , at which we obtain sheared frictionless packings with  $Z = 4$ . Thus, the sheared configurations of frictionless spheres we generate jam in the presence of friction above a threshold friction coefficient that closely matches those of frictional packings [8], above the threshold density of 0.55. Shear jammed configurations form from sheared steady state configurations with negligible rearrangement, in contrast to isotropic frictional jamming, and are anisotropic, as shown in Figure 4(d). The anisotropy (defined from the fabric tensor; see Methods) of the shear jammed configurations

is identical to the sheared steady state configurations in the range of densities where we obtain shear jamming. As an independent test, to be described elsewhere, we solve the force balance equations for the steady state configurations using the DEM generated forces as initial guesses, to obtain forces needed for force balance from geometric information alone.

Although many questions are suggested from the results above that must be investigated further, they show that shear deformation of spheres even in the absence of friction at densities well below the isotropic jamming point leads to the emergence of geometric features resembling jammed packings, with a threshold density that may be identified with the random loose packing limit that may be identified with the case of infinite friction. The force distributions and the relationship between the packing fraction and contact number in the steady state support the comparison of the sheared configurations above the threshold density with frictional jammed packings with varying friction. Our results thus serve to disentangle the role of structure formation under shear and friction in the generation of shear jamming phenomenology. They also identify the lower limit of shear jamming with random loose packing. Whether the same kind of structure formation can arise in isotropic compression[12] rather than shear, analysis of the anisotropies in sheared structures, and the role of finite shear rates present some obvious questions to pursue in future work.

### **Methods:**

The model system we study is composed of  $N = 2000$  frictionless spheres interacting with soft harmonic repulsive potential,  $v(r) = \frac{\epsilon}{2} (1 - (r/\sigma))^2$ , where  $\epsilon$  and  $\sigma$ , the interaction strength and size of the spheres, define the reduced units used throughout. The initial configurations are hard sphere configurations, obtained at high densities in two ways: (1) Starting from an equilibrated hard sphere fluid at initial density 0.45, a fast initial compression is effected using a Monte Carlo simulation till the desired density is reached for the initial configurations. (2) Starting from packings at  $\phi_j$ , obtained by the Lubachevsky-Stillinger (LS) jamming protocol [24], lower density configurations are obtained by rescaling the simulation box size. The LS procedure involves event driven molecular dynamics of hard spheres, whose radii are inflated at a specified rate. The procedure terminates when the radii cannot be increased by any finite amount without the next collision of a pair of spheres intervening, or when the collision rate diverges. In practice, the procedure is terminated when the sphere radii do not change by more than  $10^{-10}$  between successive collisions.

Athermal quasistatic simulations (AQS) are performed using LAMMPS [29], which in-

volves the following steps: (1) Affine transformation of coordinates by a small step with  $d\gamma = 5 \times 10^{-5}$ . (2) Energy minimisation using the conjugate-gradient method, employing Lees-Edwards periodic boundary conditions. This procedure is used till steady states are reached. We also use a strain step of  $d\gamma = 5 \times 10^{-12}$  to shear steady state configurations further to validate our contact definition (see below), to evaluate contact forces and to perform frictional simulations.

Data shown are averaged over 50 – 70 initial independent configurations, except Figure 4 which are averaged over 10 configurations, Figure 3 (b) which is averaged for 20 configurations and Figure 3 (d) which is averaged over 1000 configurations.

We use a cut-off of  $\sim 10^{-5}$ , which is the distance at which  $g(r)$  deviates from the power law, to define *contact* neighbours in order to compute the contact number  $Z$ . This cut-off is a precision limit that is dependent on the strain step used in AQS, as we show in SI by considering various  $d\gamma$  down to  $5 \times 10^{-12}$ . In order to have a consistent definition of contact, we compress configurations by rescaling the diameter of the spheres (by  $\sim 10^{-5}$  when  $d\gamma = 5 \times 10^{-5}$  and  $\sim 10^{-12}$  when  $d\gamma = 5 \times 10^{-12}$  etc.) so that all neighbor pairs identified as contact neighbors have finite contact forces. Since this equivalence becomes more exact for smaller strain steps, we consider steady state configurations with strain step  $d\gamma = 5 \times 10^{-12}$  when evaluating forces between contact neighbours (Fig. 3(b)). The data for frictional simulations (Fig. 4) is for  $d\gamma = 5 \times 10^{-5}$ . Data shown in the SI validate in detail the procedure we adopt.

In order to generate jammed configurations using the LS procedure, the small overlaps in the sheared configurations are removed by decreasing the diameter by a small amount ( $\sim 10^{-9}$ ) which is then increased to unity through the LS protocol with a fast compression rate of 0.1, involving negligible displacements of spheres ( $\sim 10^{-16}$ ). We use the steady state configurations to calculate free volumes of the particles using the algorithm described in [19].

To test the stability of steady state sheared structures in presence of friction, we use discrete element method (DEM) [30] to model contact interactions between particles through a repulsive linear spring-dasphpot model. The model, described further in SI, involves normal and tangential spring constants  $\kappa_n, \kappa_t$ , damping coefficients  $\zeta_n, \zeta_t = \frac{1}{2}\zeta_n$ , and the friction coefficient  $\mu$  as parameters. The model parameters used are  $\kappa_n = \kappa_t = 2$  and the normal contact damping  $\zeta_n = 0, 3, 30$ . At each contact, the Coulomb yield criterion is

obeyed i.e,  $F_t \leq \mu F_n$ , where  $\mu$  is the friction coefficient which is initially varied from .01 to 100 in multiple of 10 in order to bracket the threshold value beyond which configurations are jammed. Threshold  $\mu$  values are refined further by considering a finer grid of values. Configurations identified as jammed display a finite shear modulus, which we illustrate in one case in the SI.

Anisotropy of initial and jammed structures for isotropic and sheared steady state initial conditions is calculated, using the fabric tensor, defined as

$$\hat{R} = \frac{1}{N} \sum_{i \neq j} \frac{\mathbf{r}_{ij}}{|\mathbf{r}_{ij}|} \otimes \frac{\mathbf{r}_{ij}}{|\mathbf{r}_{ij}|} \quad (1)$$

where  $\mathbf{r}_{ij}$  are distance vectors between contact neighbors. The normalized difference between the largest eigen value  $C_1$  to the smallest  $C_3$ ,  $(C_1 - C_3)/(C_1 + C_2 + C_3)$  defines the fabric anisotropy.

- 
- [1] Liu, A. J. & Nagel, S. R. The Jamming Transition and the Marginally Stable Solid. *Annu. Rev. Condens. Matter Phys.* **1** 347-369 (2010).
  - [2] Bernal, J. D. and Mason, J. Packing of Spheres: Co-ordination of Randomly Packed Spheres, *Nature* **188**, 910 - 911 (1960).
  - [3] Scott, G. D. Packing of Spheres: Packing of Equal Spheres *Nature* **188**, 908-909 (1960)
  - [4] Torquato, S. and Stillinger, F. H. Jammed hard-particle packings: From Kepler to Bernal and beyond *Rev. Mod. Phys.* **82**, 26332672 (2010).
  - [5] Chaudhuri, P., Berthier, L., and Sastry, S. Jamming Transitions in Amorphous Packings of Frictionless Spheres Occur over a Continuous Range of Volume Fractions, *Phys. Rev. Lett.* **104**, 165701 (2010).
  - [6] O'Hern, C. S., Langer, S. A., Liu, A. J. and Nagel, S. R., Random Packings of Frictionless Particles, *Phys. Rev. Lett.* **88** 075507 (2002).
  - [7] Song, C., Wang, P. & Makse, H. A. A phase diagram for jammed matter. *Nature* **453**, 629-632(2008).
  - [8] Silbert, L. E. Jamming of frictional spheres and random loose packing, *Soft Matter* **6**, 2918-2924(2010).
  - [9] Bi, D., Zhang, J., Chakraborty, B. & Behringer, R. p. Jamming by shear. *Nature* **480**, 355-



- 358(2011).
- [10] Otsuki, M. and Hayakawa, H. Critical scaling near jamming transition for frictional granular particles. *Phys. Rev. E*, **83** 051301 (2011).
  - [11] Ciamarra, P., Pastore, R., Nicodemi, M. and Coniglio, A. Jamming phase diagram for frictional particles. *Phys. Rev. E*, **84** 041308 (2011).
  - [12] Shen, T., O'Hern, C. S. and Shattuck, M. D. Contact percolation transition in athermal particulate systems **85** 011308 (2012).
  - [13] Heussinger, C. and Barrat, J.-L. Jamming Transition as Probed by Quasistatic Shear Flow *Phys. Rev. Lett.* **102** 218303 (2009).
  - [14] Onoda, G. Y. & Liniger, E. G. Random loose packings of uniform spheres and the dilatancy onset. *Phys. Rev. Lett.* **64**, 2727-2730 (1990).
  - [15] Bertrand, T. *et al* Protocol dependence of the jamming transition, arXiv:1506.05041.
  - [16] Kumar, N. and Luding, S. Memory of jamming - multiscale flow in soft and granular matter. arXiv:1407.6167.
  - [17] O'Hern, C. S., Silbert, L. E., Liu, A. J & Nagel, S. R. Jamming at zero temperature and zero applied stress: The epitome of disorder. *Phys. Rev. E*. **68**, 011306(2003).
  - [18] Donev, A., Torquato, S., & Stillinger, F. H. Pair correlation function characteristics of nearly jammed disordered and ordered hard-sphere packings. *Phys. Rev. E*. **71** , 011105(2005).
  - [19] Maiti, M. and Sastry, S. Free volume distribution of nearly jammed hard sphere packings. *J. Chem. Phys.* **141**, 044510 (2014).
  - [20] Maiti. M., Vinutha, H. A., Heussinger, C. and Sastry, S. Free Volume under Shear, *J. Chem. Phys.* (in press).
  - [21] O'Hern, C. S., Langer, S. A., Liu, A. J. and Nagel, S. R., Force Distributions near Jamming and Glass Transitions, *Phys. Rev. Lett.* **86** 111-114 (2001).
  - [22] Wyart, M. Marginal Stability Constrains Force and Pair Distributions at Random Close Packing *Phys. Rev. Lett.* **109** 125502 (2012).
  - [23] Lerner, E., Dřuing, G. and Wyart, M. Low-energy non-linear excitations in sphere packings *Soft Matter* **9**, 8252-8263 (2013).
  - [24] Lubachevsky, B. D. & Stillinger, F. H. Geometric properties of random disk packings. *J. Stat. Phys.* **60**, 561-583(1990).
  - [25] Speedy, R. J. The hard sphere glass transition. *Mol. Phys.* **95**, 169-178(1998).

- [26] Brown, E. & Jaeger, H. M. Dynamic jamming point for shear thickening Suspensions. *Phys. Rev. Lett.* **103**, 086001(2009).
- [27] Cates, M. E., Wittmer, J. P., Bouchaud, J.-P. and Claudin, P. Jamming, Force Chains, and Fragile Matter. *Phys. Rev. Lett.* **81**, 1841 (1998).
- [28] Henkes, S., van Hecke, M. and van Saarloos, V. Critical jamming of frictional grains in the generalized isostaticity picture *Euro Phys. Lett.* **90** 14003 (2010).
- [29] Plimpton, S. Fast Parallel Algorithms for Short-Range Molecular Dynamics. *J. Comput. Phys.* **117** 119 (1995).
- [30] Cundall, P. A. & Strack, O. D. L. A discrete numerical model for granular assemblies. *Geotechnique* **29**, 4765 (1979).

We wish to thank S. S. Ashwin, Bulbul Chakraborty, Corey O’Hern, Stefan Luding, Itamar Procaccia and Sidney Nagel for useful discussions. We gratefully acknowledge the use of computational resources at TUE-CMS, JNCASR, Bangalore and TCIS, TIFR Hyderabad. This research was supported in part by the National Science Foundation under Grant No. NSF PHY11-25915.

## Figure Captions

**Figure 1 :** (a) Evolution of radial distribution function  $g(r)$  for  $\phi = 0.58$  with strain ( $\gamma$ ). For  $\gamma = 0.41$ , the system has reached the steady state and has a power law in  $g(r)$  extending over 5 decades. (b) Radial distribution function showing changes in the second peak as the system is strained. As we move from the bottom curve to the top curve, the direction of increase in strain, the discontinuity in the second peak develops and becomes stronger. Each curve are shifted from by 1 from the previous along the  $y$  axis for clarity. (c) Distribution of contact number as a function of strain. At zero strain, there are no contact neighbours and after  $\gamma = 0.1$ , particles begin to have contact neighbours. (d) Evolution of the free volume distribution with strain. The power law tail in  $f(V_f)$  develops around the same strain value for which contact neighbour distribution develops a peak at a non zero value of  $Z$ . Data for nearly jammed configurations at 0.639 are shown in all panels for comparison (thick green lines).

**Figure 2 :** (a) Power law divergence in  $g(r)$  for sheared configurations in the steady state. The power law exponent value depends slightly on density and is about 0.45 for the nearly jammed case. (b) Singularities in the second peak of the  $g(r)$  are observed at all densities at  $\sqrt{3}\sigma$  and  $2\sigma$ , with the feature at  $\sqrt{3}\sigma$  becoming stronger as density increases. (c) Distribution of contact number. (d) Free volume distributions. The exponent of the power law tail indicated by fit lines depends on slightly on density. Data for nearly jammed configurations at 0.639 are shown in all panels for comparison (thick green lines).

**Figure 3 :** (a) Parametric plot showing the average contact number *vs.* density for sheared configurations, compared with that of frictional packings obtained by Song et al [7] and Silbert [8]. The average contact number becomes greater than 4 for  $\phi \geq 0.55$ . (b) The distribution of contact forces for different densities which show a peak at finite values for  $\phi \geq 0.55$ . (c) Configurations subjected to the LS jamming protocol at different compression rates. Plotted are the resulting densities of jammed configurations indicating a change of behaviour for  $\phi > 0.58$ . Compression rates in the legend are indicated by "CR". (d) Percolation of jammed ( $Z \geq 2D$ ) spheres in the sheared configurations indicating a percolation threshold at  $\phi = 0.585$ , shown for different system sizes.

**Figure 4 :** (a) Threshold friction coefficient as a function of the density, beyond which sheared steady state structures jam, for damping coefficients  $\zeta_n = 0, 3, 30$ . Also shown for comparison are results for frictional packings obtained by Silbert [8]. (b) Fraction of contact pairs initially present that survive as a function of time, for the threshold friction coefficient (for density  $\phi \geq 0.59$ ; for  $\phi = 0.55$  and  $0.58$  the friction coefficient is 10), and  $\zeta_n = 0$ . (c) Comparison of coordination number  $Z$  of the initial structure and the final structure obtained from frictional dynamics after applying a strain of  $\Delta\gamma = 5 \times 10^{-5}$ . Curves labeled  $\zeta_n = 0, 3, 30$  are for steady state configurations with  $d\gamma = 10^{-5}$ , just above the threshold friction coefficient, and no solvent friction, whereas configurations for the curve labeled  $\zeta_n = 3, \eta = 3$  are obtained with  $d\gamma = 10^{-12}$ , for friction coefficients well above threshold, and finite solvent friction  $\eta$ . The contact number is close to, but different from, the initial value for densities above  $\phi = 0.57$ , whereas they are zero for lower densities (except the case  $\zeta_n = 3, \eta = 3$ , where overdamping results in cessation of particle motion before all contacts are lost). (d) Fabric anisotropy as a function of packing density for steady state (SS), shear jammed (SJ) and isotropic frictional jammed (ISO) configurations. The anisotropy of SS and SJ packings are same.

TABLE I. Statistics of steady state structural features of sheared packings.  $\phi$  is the density of sheared packings,  $\langle Z \rangle$  and  $\langle Z_{NR} \rangle$  is the average coordination number with and without rattlers, and RP is the rattler ( $Z \leq 3$ ) percentage.  $Q_6$  is the global bond orientational parameter computed to check absence of crystallinity.

$\phi$	0.45	0.5	0.54	0.56	0.58	0.59	0.61	0.627
$\langle Z \rangle$	2.54	3.23	3.88	4.24	4.615	4.81	5.26	5.65
$Q_6$	0.049	0.054	0.052	0.038	0.028	0.027	0.025	0.023
RP	0.795	0.572	0.358	0.262	0.175	0.138	0.078	0.037
$\langle Z_{NR} \rangle$	4.2	4.38	4.63	4.82	5.042	5.175	5.495	5.785

# Figures

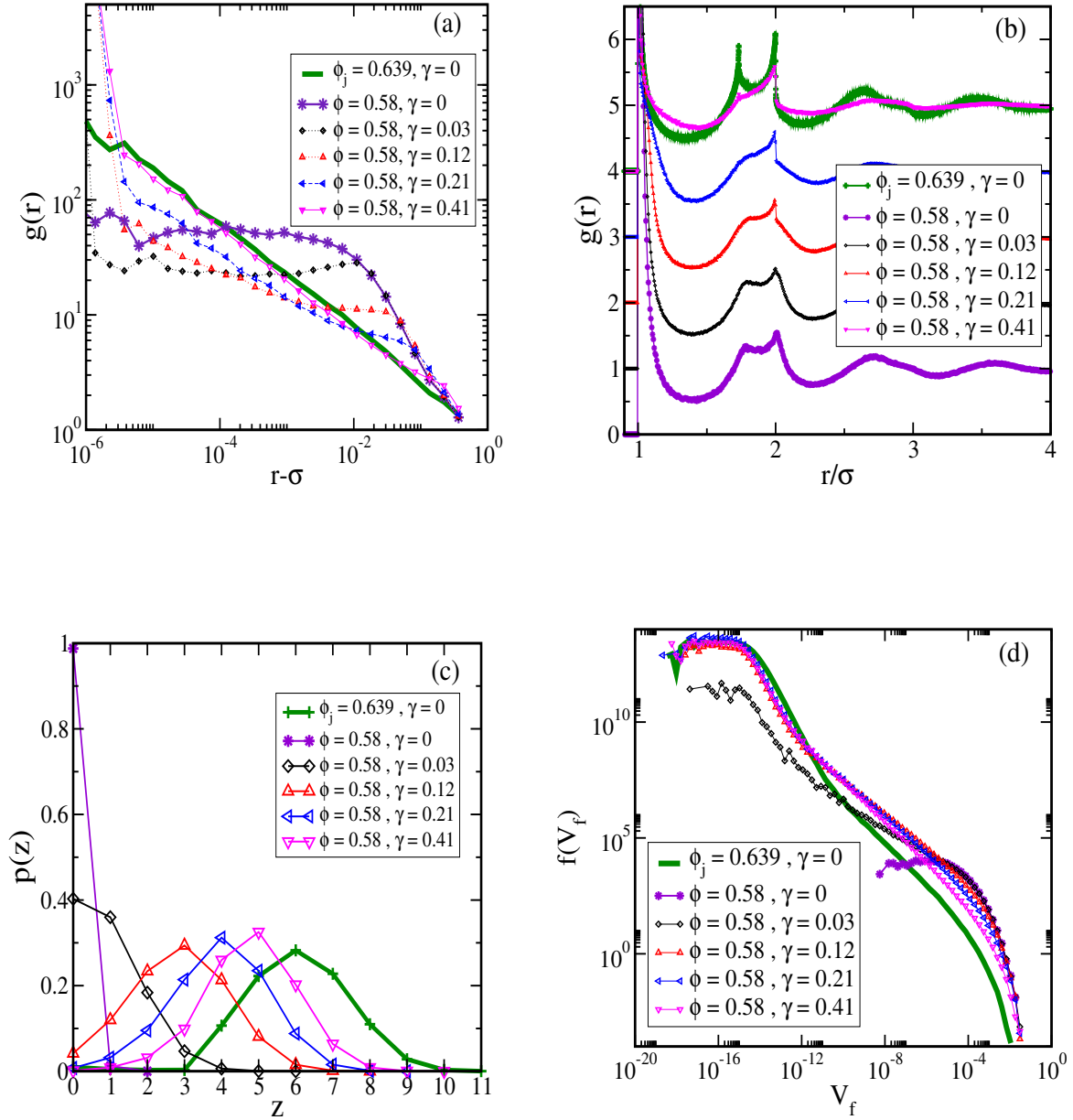


FIG. 1.

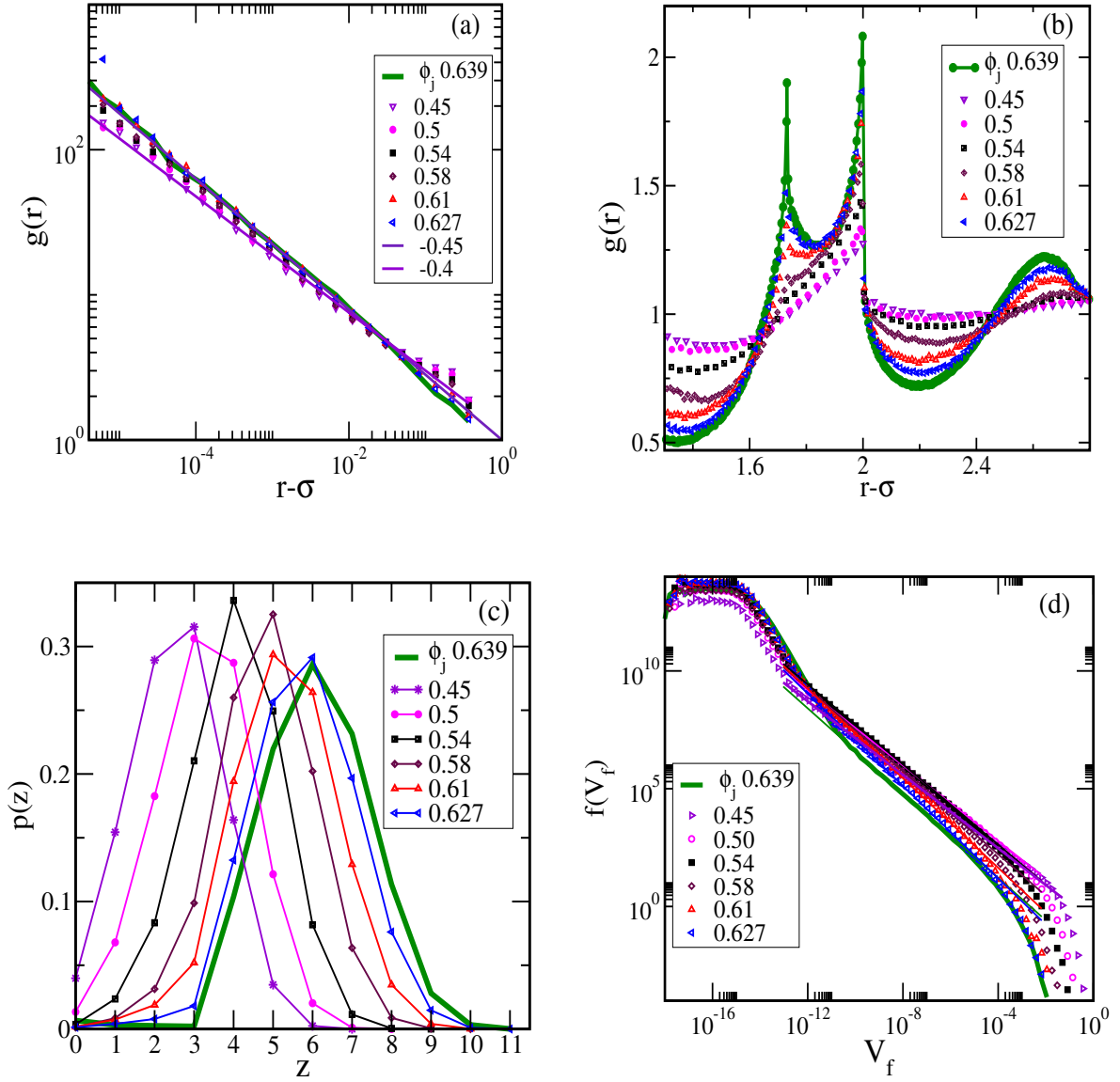


FIG. 2.

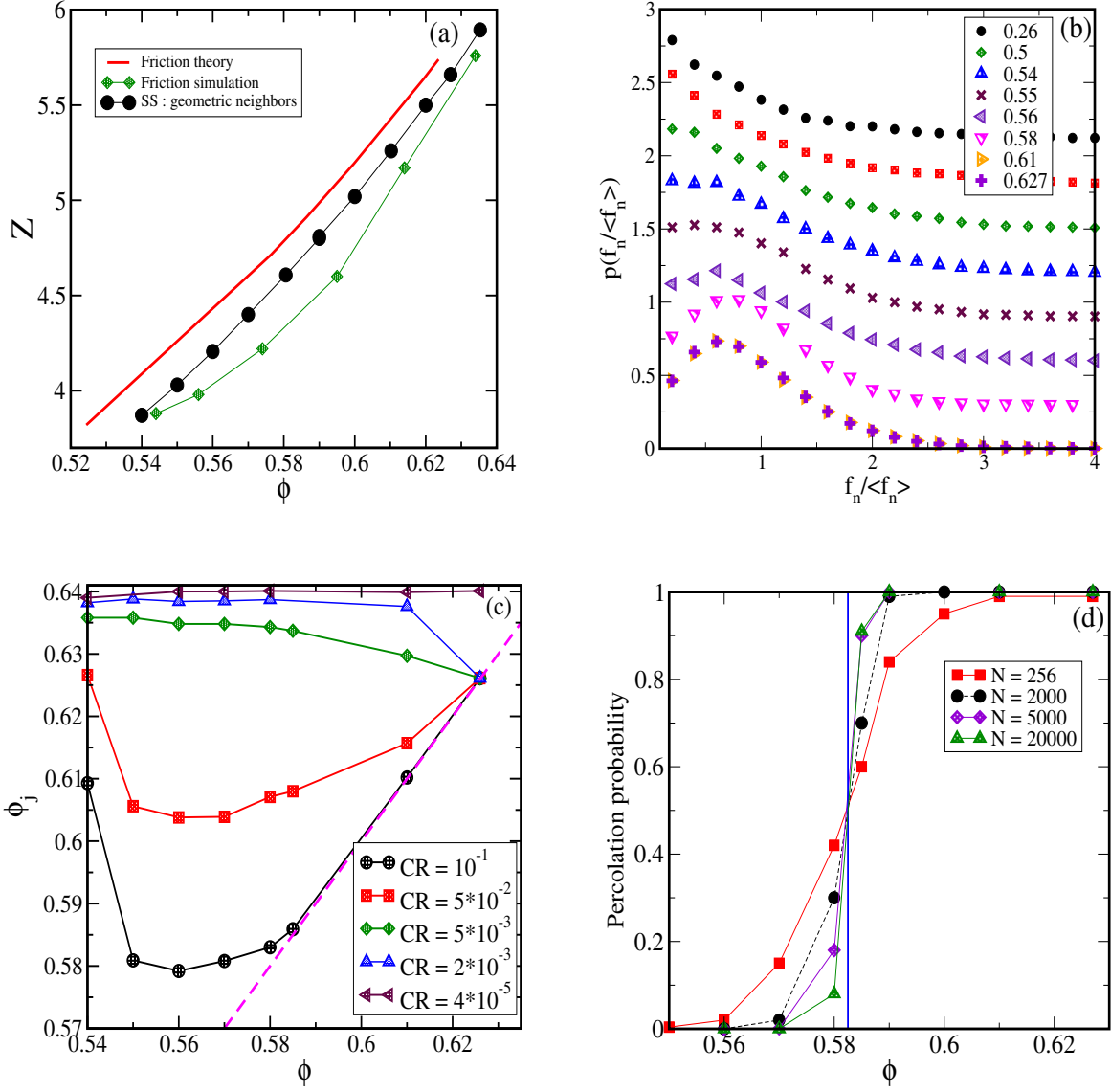


FIG. 3.



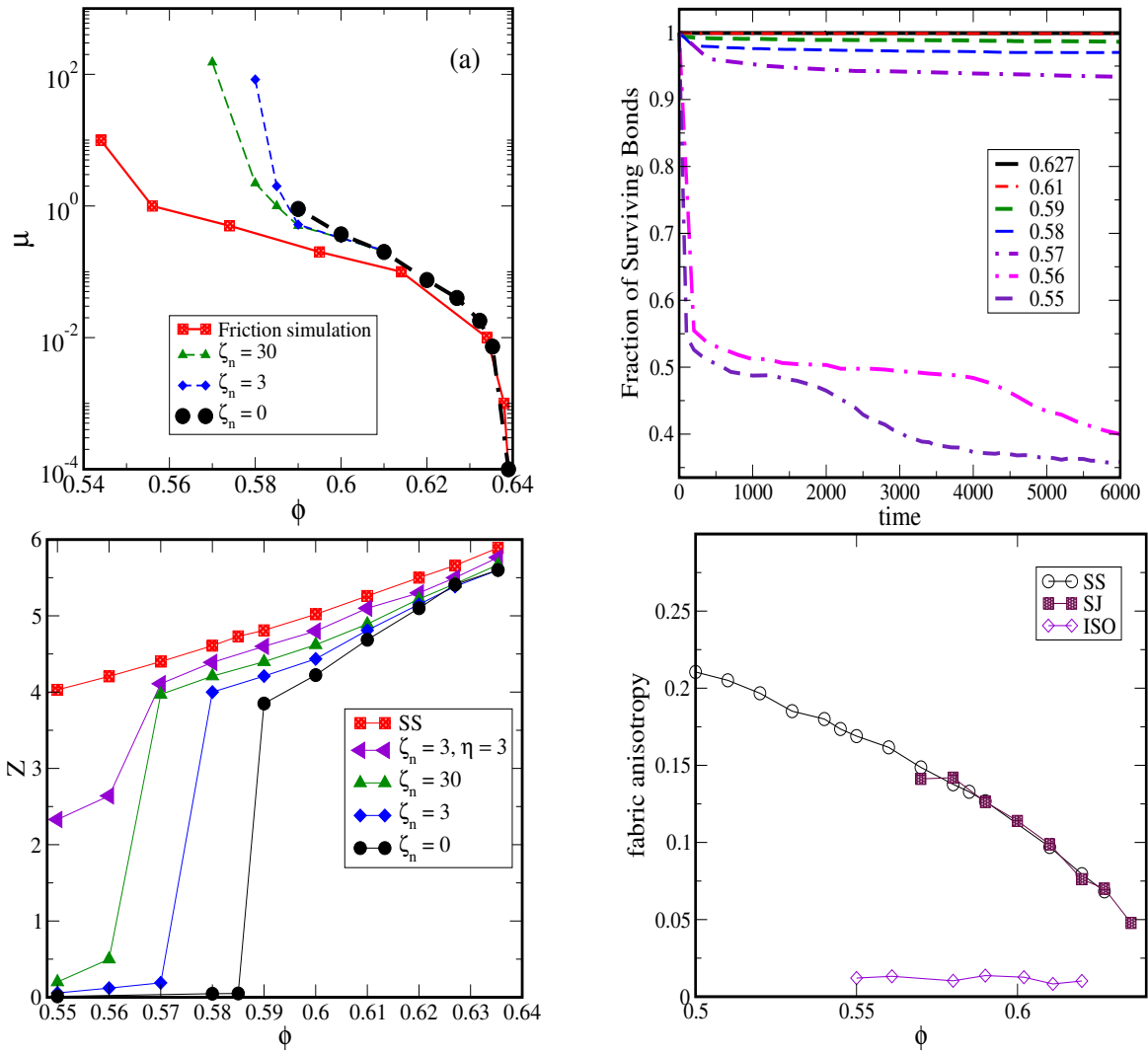


FIG. 4.

# Disentangling the role of structure and friction in shear jamming

## (Supplementary Information)

H.A. Vinutha and Srikanth Sastry

Here we present additional information regarding three aspects of our analysis of sheared sphere configurations, namely: (i) Approach to the steady state, (ii) Evaluation of the contact number, and (iii) Determination of the lower limit of shear jamming in the presence of friction.

### I. APPROACH TO THE STEADY STATE

The analysis we present is performed for steady state configurations. Whether the simulated system has reached steady state or not is assessed by monitoring various structural and dynamic quantities, which show behavior consistent with the average contact number and the shear stress. Because the stresses are negligible for energy minimum configurations, we calculate stresses for configurations before minimization in the AQS protocol. The average contact number (whose evaluation is discussed next) and shear stress reach steady state values beyond strain values that depend on the density (Fig. 5).

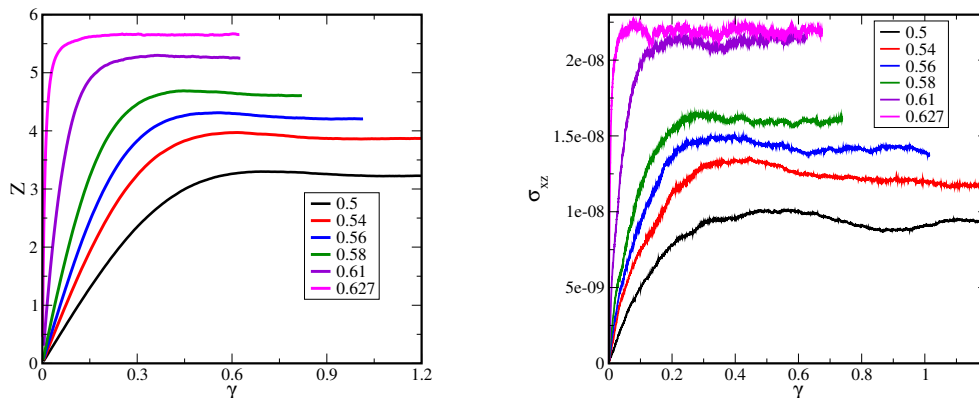


FIG. 5. (a) Coordination number  $Z$  as a function of strain for different densities. The value of  $Z$  and the strain value where the steady state is reached depends on density. (b) Stress in the shear plane as a function of strain for different densities. The strain values at which steady state stress is reached compares well with the corresponding values for the coordination number  $Z$ .

## II. EVALUATION OF THE CONTACT NUMBER $Z$

In our analysis, we determine the contact number geometrically in the first instance, from the pair correlation function  $g(r)$ . As seen in Fig. 6(a), the pair correlation function exhibits a deviation from the power law form at small distances (below  $r - \sigma = 10^{-5}$ ). We identify the contact neighbors as those at distances  $r - \sigma < tol$  where  $tol$  is the value where the near contact  $g(r)$  deviates from the power law behavior. We attribute the fact that these contact distances are not exactly equal to  $\sigma$  to the finite precision of the procedure used to generate the configurations. With that premise, the use of a tolerance  $tol$  is a reasonable procedure to identify contact neighbors, but such neighbors will not necessarily be *in contact*, *i. e.* exert a finite force on each other. This limitation can be overcome by compressing the sphere together such that all spheres within  $\sigma + tol$  come in to contact with each other. We use such a procedure in our work when evaluating forces and in performing frictional simulations. Here, we validate these procedures. In order to do so, we first show that the deviation from the power law occurs for distance values that depend systematically on the precision of the numerical procedure used. In the case of the athermal quasistatic procedure we use, the limit to precision arises from the finite strain steps  $d\gamma$  used. We next show that in the limit of vanishing  $d\gamma$ , the average number of contacts, defined as pairs of spheres exerting forces on each other, becomes equal to the average number of *geometric* neighbors we identify from the  $g(r)$ .

We generate steady state sheared configurations for different values of the strain step  $d\gamma$ , by starting from the steady state configurations with  $d\gamma = 5 \times 10^{-5}$ , and progressively decreasing  $d\gamma$ , and obtaining the corresponding steady state configurations. As shown from Fig. 6 (a) the location of the departure from the power law ( $tol$ ) depends on the  $d\gamma$  value. In Fig. 6 (b) - (d) we show the cumulative distribution of neighbors,  $Z(r)$ , defined as the number of neighbors of a given sphere within a distance  $r$ . The behavior of  $Z(r)$  for different values of  $d\gamma$  shows clearly that in the limit of  $d\gamma \rightarrow 0$ , the plateau value of  $Z(r)$ , which corresponds to counting neighbors within  $\sigma + tol$  with  $tol$  identified from the  $g(r)$ , becomes exact as the number of contact neighbors. Thus, for finite strain step simulations, (a) counting the *geometric* neighbors defined from  $g(r)$  as above as contact neighbors, and (b) compressing the configurations to induce contact between neighbors at distances below  $\sigma + tol$  when forces and dynamics are studied, are both seen to be reasonable. We use these procedures,

but to minimize the approximation to the AQS procedure as much as possible, consider the case of  $d\gamma = 5 \times 10^{-12}$  when evaluating forces, and performing frictional simulations.

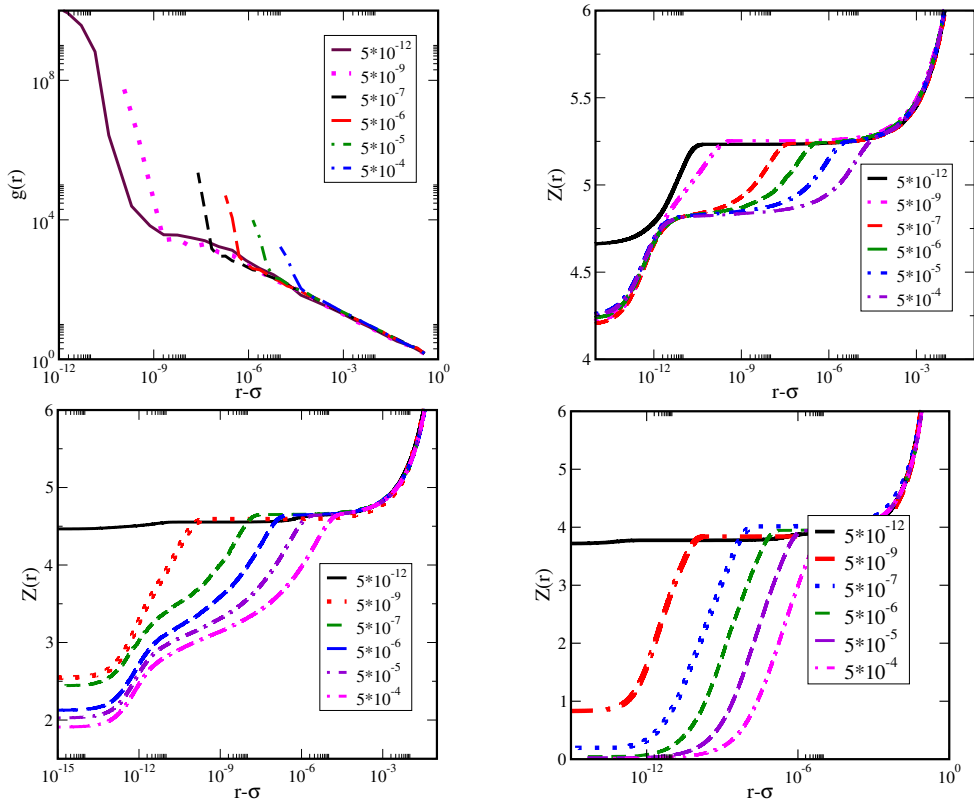


FIG. 6. (a) Radial distribution function for  $\phi = 0.61$  for different values of strain step. The distance at which a departure from the power law in  $g(r)$  is seen depends on the strain step used in shearing. Cumulative distribution of neighbor number shown for different  $d\gamma$  for (b)  $\phi = 0.61$ , (c)  $\phi = 0.58$ , and (d)  $\phi = 0.54$ . The plateau value is the same for all  $d\gamma$  values to a very good degree. In the limit of  $d\gamma \rightarrow 0$ , the plateau in  $Z(r)$  extends to  $r = \sigma$ , indicating that the unique contact number in that limit is reliably obtained by considering the plateau value when performing finite  $d\gamma$  shearing.

### III. LOWER LIMIT FOR SHEARING JAMMING IN THE PRESENCE OF FRICTION

Here, we provide details of these procedures we use to identify the lowest friction coefficient for which sheared steady state configurations jam, and thereby, how we identify the lower density limit to frictional jamming.

We used the discrete element method to simulate frictional interactions between the spheres. A linear-spring dashpot model is used with forces between particles in contact given by

$$\vec{F} = (\kappa_n \delta n_{ij} - m_{eff} \zeta_n \vec{v}_n) - (\kappa_t \Delta s_t + m_{eff} \zeta_t \vec{v}_t). \quad (2)$$

The first term in the normal force between the two particles and the second term is the tangential force.  $\kappa_n$  and  $\kappa_t$  is the elastic constant for normal and tangential displacements.  $\zeta_n$  and  $\zeta_t$  are damping constants for the normal and tangential contacts.  $m_{eff}$  is the effective mass of the spheres.  $\Delta s_t$  is the tangential displacement vector between two spheres from the contact point.  $n_{ij}$  is the unit vector along the line connecting the centers of the two particles and  $\delta n_{ij}$  is the normal displacement of the spheres (towards each other) from the contact position.  $v_n$  and  $v_t$  are the normal and tangential components of the relative velocity of the two particles. The maximum value of the tangential force  $F_t$  follows the Coulomb criterion,  $F_t \leq \mu F_n$ , where  $F_n$  is the normal force, and  $\mu$  is the friction coefficient. We also include solvent friction in some cases, through a frictional force term  $\vec{F}_{solvent} = -\eta \vec{v}$ .

The input parameters used in our analysis is  $\kappa_n = \kappa_t = 2$ ,  $\zeta_n = 0, 3, 30$  and  $\zeta_t = \frac{1}{2} \zeta_n$ . We use sheared steady state structures, compressed by  $tol$  to form all the contacts that are counted (see previous section) and strained by a variable step  $\Delta\gamma$ , as initial configurations. Stability of the sheared structures are tested by applying strain steps  $\Delta\gamma$  in the range  $0-10^{-2}$  and allowing the system to relax. By varying the friction coefficient, we identify, for each density, the friction coefficients for which the initial structure remains stable. Fig. 7 shows that for  $\phi = 0.627$ , the packings have finite stress and contact number after applying a strain step of  $\Delta\gamma = 5 * 10^{-5}$  for a range of friction coefficients. The decay or otherwise of the shear stress, and the contact number provide clear and consistent criteria for judging whether the system remains jammed for a given friction coefficient  $\mu$ . For  $\phi = 0.58$ , shown in Fig. 8, the stresses and contact numbers decay to zero for all the friction coefficients studied, and thus in this range of  $\mu$ , the system does not jam. It appears that the limit value in density for any friction coefficient will also depend on other parameters, namely the damping coefficients. Fig. 9 shows the same data for  $\phi = 0.58$ , but for a damping coefficient of  $\zeta_n = 3$ , which indeed shows that for finite damping, the system is jammed above a threshold friction coefficient.

In Fig. 10, we show the percolation of spheres with  $D+1$  contacts, such that the contacts

are not all in the same half space with respect to the central sphere, for different system sizes. It is seen that the percolation transition occurs at density  $\phi = 0.53$ . This threshold is a little lower than  $\phi = 0.55$  where we see other indications of a change in behavior, and its significance remains to be understood better.

Finally, we consider the stress the jammed structures should experience at the end of the relaxation. For jammed configurations, one should expect a linear stress-strain dependence, resulting in a finite shear modulus from the slope of the stress-strain curve. However, since the frictional dynamics is initiated after a compression that is determined by the strain step  $d\gamma$ , the jammed packings exhibit an initial stress value that is independent of the strain  $\Delta\gamma$ . To demonstrate that this is an artefact of finite precision, we consider steady state configurations obtained with different  $d\gamma$ , and consider the final stress-strain curves *vs.*  $\Delta\gamma$ . We see, in Fig. 11, that as  $\Delta\gamma$  exceeds  $d\gamma$ , we obtain a linear stress-strain relation, from which a modulus may be extracted.

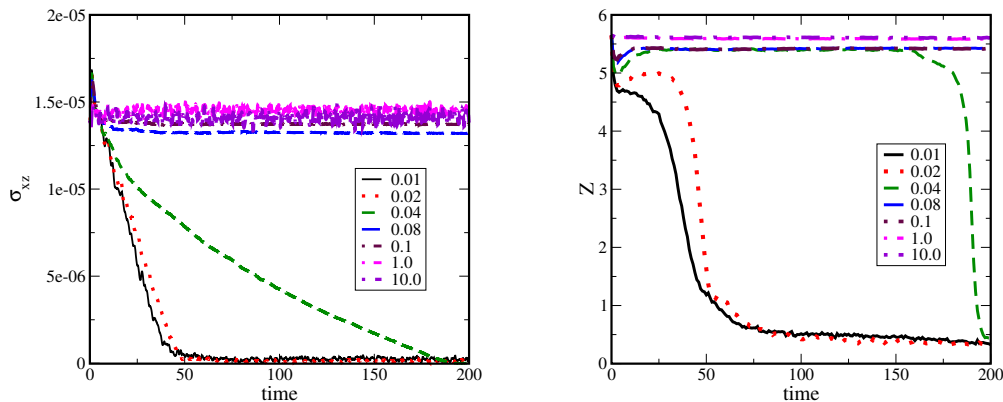


FIG. 7. For  $\phi = 0.627$ , **(a)** stress, and **(b)** contact number, as function of time for the sheared configurations after an initial strain of  $\Delta\gamma = 5 \times 10^{-5}$  for different friction coefficients. For very low friction coefficient, the shear stress relaxed to zero indicating that the structure is jammed, whereas the stress remains finite for large friction coefficients indicating that the structure is jammed. Similarly, the contact number decays to zero for structures that are not stable, while remaining close to the initial value for jammed structures.

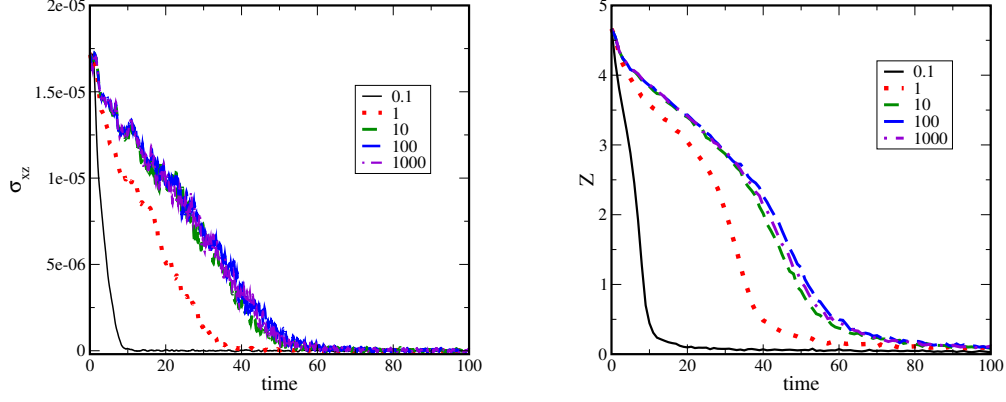


FIG. 8. For  $\phi = 0.58$ , (a) stress, and (b) contact number, as function of time for the sheared configurations after an initial strain of  $\Delta\gamma = 5 \times 10^{-5}$  for different friction coefficients. Neither the stress nor contact number remain finite for any friction coefficients, indicating that the structures are not stable in the studied range of friction.

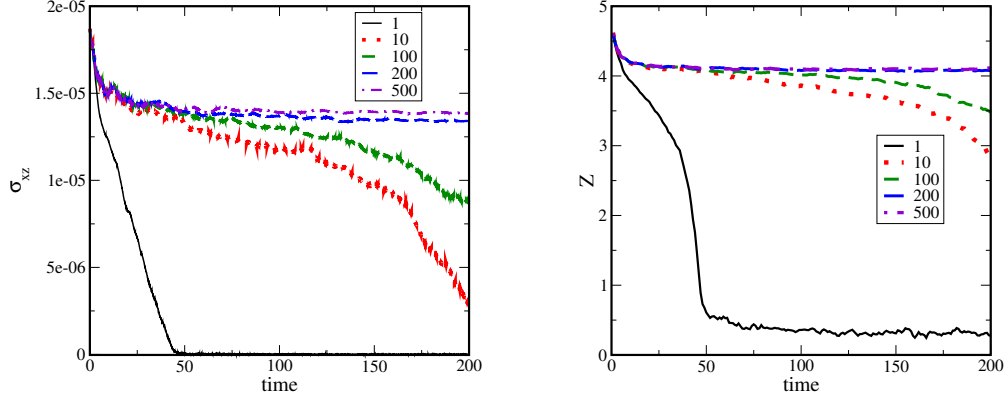


FIG. 9. For  $\phi = 0.58$ , (a) stress, and (b) contact number, as function of time for the sheared configurations after an initial strain of  $\Delta\gamma = 5 \times 10^{-5}$  for different friction coefficients with normal damping constant  $\zeta_n = 3$ . The stress and contact number remain finite for high friction coefficients, indicating that the structures can be stabilized by adding small amount of damping.

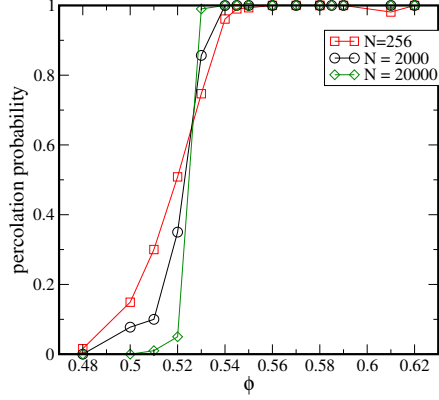


FIG. 10. Percolation of spheres with  $D + 1$  contacts, such that all the neighbors are not on the same half space with respect to the central sphere.

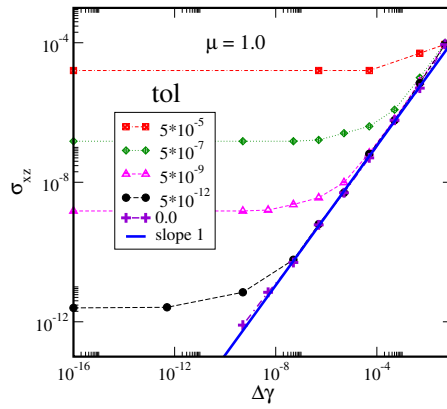


FIG. 11. Stress as a function of applied strain  $\Delta\gamma$  for  $\phi = 0.61$  and  $\mu = 1.0$ , shown for configurations obtained using different strain steps  $d\gamma$ . The initial sheared configurations are compressed by an amount  $tol$  that depends on  $d\gamma$  to include all the contacts before the strain  $\Delta\gamma$  is applied. For  $\Delta\gamma > tol$ , the shear stress is proportional to strain as expected for an elastic solid.